POLITECNICO DI TORINO
Repository ISTITUZIONALE

Non-equilibrium Scaling of the Turbulent-Nonturbulent Interface Speed in Planar Jets

(Article begins on next page)

03 May 2024

Nonequilibrium Scaling of the Turbulent-Nonturbulent Interface Speed in Planar Jets

Gioacchino Cafiero [1,*] and J. Christos Vassilicos [2,†]

[1]*Centre for Aerodynamics and Environmental Flow, Department of Mechanical Engineering Sciences, University of Surrey, GU2 7HX Guildford, United Kingdom*
[2]*Université Lille, CNRS, ONERA, Arts et Metiers Institute of Technology, Centrale Lille, UMR 9014—LMFL—Laboratoire de Mécanique des fluides de Lille–Kampé de Feriet, F-59000 Lille, France*

The length scale which, combined with the fluid's kinematic viscosity ν, defines the local average speed of the turbulent-nonturbulent interface has been postulated to be the smallest (Kolmogorov) length scale η of the turbulence Corrsin and Kistler, [NACA Report No. 1244, 1955, p. 1033.]. This is indeed the case when the turbulence dissipation rate obeys the Kolmogorov equilibrium cascade scaling, but in the presence of the nonequilibrium turbulence dissipation scaling the average local turbulent-nonturbulent interface speed scales as ν/λ, instead of ν/η, where λ is the Taylor length. We derive this theoretically and confirm it experimentally in the range of distances between 20 and 50 nozzle widths of a turbulent planar jet.

Interfaces are essential paradigmatic phenomena in nonequilibrium statistical physics which appear in a wide range of physical and physicochemical contexts. The turbulent-nonturbulent interface (TNTI) is one important example of interfaces which encapsulates one of the greatest challenges in statistical physics and turbulence research: how to make sense of turbulence dynamics in the absence of homogeneity and isotropy. The TNTI is a sharp and convoluted fluctuating layer between potential non-turbulent flow on one side and vortical turbulent flow on the other. It exists at the edge of a very wide range of turbulent flows including turbulent boundary layers, jets, plumes, wakes, and mixing layers, and is of central relevance to mixing of mass and momentum in many environmental, geophysical and industrial contexts including combustion and cloud physics [1,2].

The TNTI's motion relative to the fluid is intimately linked to entrainment. In fact, the rate at which fluid without vorticity is entrained into the turbulent core of the flow and acquires vorticity depends on the local speed of the interface relative to the fluid and on the interface's area per unit volume [1,3]. These two TNTI properties, local speed and area per unit volume (or length per unit area in a planar cut through the flow), are therefore key to understanding and modeling entrainment, mass, and momentum fluxes.

Corrsin and Kistler [4] advanced the idea that the local speed of the TNTI scales with the characteristic velocity of the smallest turbulence eddies, i.e., the Kolmogorov velocity ν/η where ν is the fluid's kinematic viscosity and η is the Kolmogorov length scale. Supporting evidence was found for this hypothesis in laboratory experiments and direct numerical simulations of turbulent flows where the Taylor

length Reynolds number Re_λ (a measure of the ratio of inertial to viscous forces) is below 100 ([5,6]). Sreenivasan *et al.* [3] obtained evidence showing that the TNTI has fractal properties and a fractal dimension equal to $7/3$, thus suggesting the possibility of an asymptotically infinite TNTI area per unit volume as the Reynolds number tends to infinity. In this limit, the local speed of the TNTI tends to 0 if it scales with the Kolmogorov velocity. As a result, the mass flux across the interface is finite and in fact sizeable even if the local speed is very small.

A few years ago, Zhou and Vassilicos [7] showed that the scalings of the local TNTI speed and the turbulence dissipation are related in the case of a self-similar turbulent axisymmetric wake in a way that is more general than envisaged in [4]. On account of the self-similarity, the wake width growth and the velocity deficit decay are determined by mass, momentum, and turbulent kinetic energy balances and the turbulence dissipation rate is an important contributor to the latter balance [8,9]. Different turbulence dissipation scalings lead to different wake width growth rates, and as pointed out in [7], this in turn means different local TNTI speed scalings. If the turbulence dissipation scaling is the one implied by the Kolmogorov equilibrium cascade, then the TNTI speed scales with the Kolmogorov velocity (as suggested in [4]) provided that the TNTI's fractal dimension is the one found in [3]; but if the turbulence dissipation obeys the nonequilibrium scaling discovered in various turbulent flows over the past ten years [8–14], then the local speed of the TNTI scales with the Taylor velocity ν/λ (where λ is the Taylor length scale) irrespective of the TNTI's fractal dimension. The potential relevance of the Taylor length scale to the TNTI's inner structure has also been pointed out in [15–17] but without
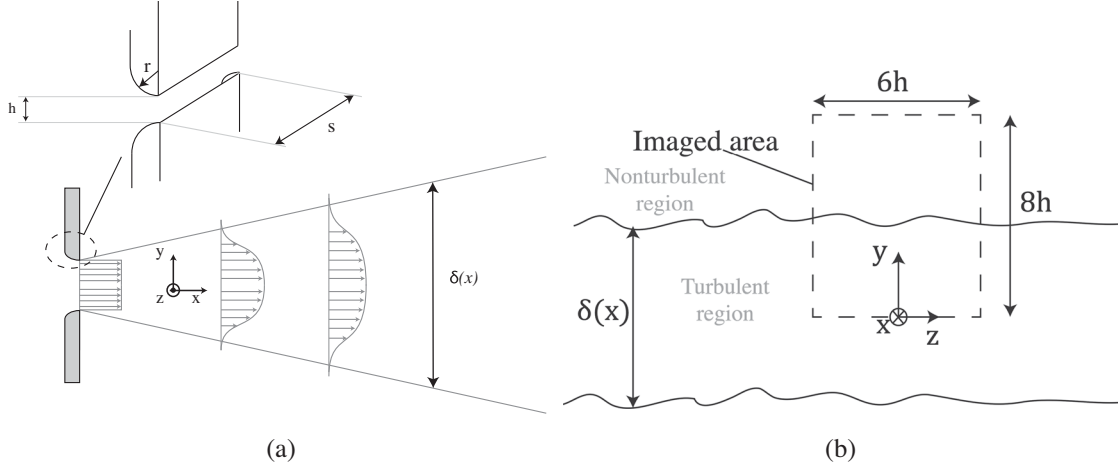
FIG. 1. (a) Schematic representation of the jet flow; (b) cross section of the jet flow with indication of the imaged area $0 \leq y \leq 8h$, $-3h \leq y \leq 3h$. The two wiggly lines at the top and bottom represent the intersection of the TNTI with the y-z plane at position x.

reference to nonequilibrium turbulence cascade and dissipation.

Evidence for the nonequilibrium dissipation scaling has been found in axisymmetric wakes [8,9,11] and planar jets [14] for values of $\mathrm{Re}_\lambda \equiv \sqrt{K_0}\lambda/\nu$ (K_0 is the turbulent kinetic energy on the centreline at $y = z = 0$), larger than 100. How does the local TNTI speed scale in the region of a planar jet where self-similarity coexists with the non-equilibrium scaling? Can the prediction made for axisymmetric turbulent wakes by [7] also be made for turbulent planar jets, namely that the local TNTI speed scales with the Taylor velocity in this region, and can such a prediction be verified experimentally? These are the main questions we answer in this Letter.

Figure 1(a) is a schematic of the main features of our experimental planar jet setup where $h = 15$ mm, $r = 2h$, $s/h = 31$, and the jet inlet velocity U_J is such that the global Reynolds number $\mathrm{Re} \equiv U_J h/\nu$ is 20 000. More details can be found in [14] who used the exact same facility at the same Re. The jet width $\delta(x)$ at streamwise position x is based on the self-similar profile of the mean streamise velocity $\langle u \rangle(x, y) = u_0(x)f[y/\delta(x)]$ where the brackets indicate a time average. Self-similarity holds for $x \geq 18h$, and statistics are homogeneous in the z direction [14]. The nonequilibrium dissipation scaling that is present in turbulent planar jets was confirmed in the present jet in the range $20h \leq x \leq 50h$ where Re_λ was found to increase from 250 to 430 [14]. The region $20h \leq x \leq 50h$ is therefore appropriate for our experiment as it combines self-similarity, large enough values of Re_λ and the nonequilibrium scaling $\varepsilon_0 \sim U_J h K_0/\delta$ where $\varepsilon_0(x)$ is the turbulence dissipation rate on the centerline $y = z = 0$.

The wiggly lines in Fig. 1(b) represent the intersection of the TNTI with the $y - z$ plane at a streamwise distance x from inlet. The turbulent region lies between these two lines and the area imaged by our particle image velocimetry (PIV) is shown too.

The following relation holds for both wakes and jets [7]:

$$\frac{d}{dx}\left\langle \int_{\mathcal{A}_t(x)} u\,dy\,dz \right\rangle = \mathcal{L}\bar{v}_n \qquad (1)$$

where, in the case of a planar jet [see Fig. 1(b)], $\mathcal{A}_t(x)$ is the instantaneous area in the $y - z$ plane at x between the upper and the lower TNTI line intersections of the TNTI in a region $-Z \leq z \leq Z$ of that plane (for Z/h large enough); $\mathcal{L}$ is the time-averaged length of the TNTI's intersection with this plane in this same region; and $\bar{v}_n \equiv \langle \int_{\partial\mathcal{A}_t(x)} v_n\,dl \rangle/\mathcal{L}$ where v_n is the local (in space and time) propagation speed of the TNTI relative to the fluid and the line integration is over the line boundary of $\mathcal{A}_t(x)$ in the region $-Z \leq z \leq Z$ of the $y - z$ plane at x. It is also worth explicitly mentioning that Eq. (1) holds for any definition of an isoline representing the TNTI.

The underlying concept in Eq. (1) is that the mean entrainment at the TNTI is directly related to the stream-wise variation of the mass flux. The use of this equation to determine the characteristic TNTI speed $\bar{v}_n$ requires knowledge of $\mathcal{L}$, and we know from [3] that the interfacial line between turbulent and non turbulent regions is fractal. We therefore write $\mathcal{L} \sim 2Z(\eta_I/\delta)^{1-D}$ in terms of the fractal dimension $1 \leq D < 2$ and the smallest length scale η_I on the interface. At this point, like in [7] for wakes, we follow Corrsin [4] and assume $\eta_I \sim \nu/\bar{v}_n$ without, however, specifying the scaling of $\bar{v}_n$. Using self-similarity, the left-hand side of Eq. (1) scales as $(d/dx)(u_0\delta Z)$ and with our expression for $\mathcal{L}$, Eq. (1) implies

$$\bar{v}_n \sim \left(\frac{\delta}{\nu}\right)^{(1-D)/D}\left(\frac{d}{dx}(u_0\delta)\right)^{1/D}. \qquad (2)$$

The mass, momentum and turbulent kinetic energy balance analysis of [14] for a self-similar planar jet showed

that $u_0 \sim (x-x_0)^{-a/2}$ and $\delta \sim (x-x_0)^a$ where $a = (m+1)/(2m+1)$ in terms of the turbulence dissipation exponent m in $\varepsilon_0 \sim (U_J h/\sqrt{K_0}\delta)^m (K_0^{3/2}/\delta)$. The classical dissipation scaling corresponds to $m = 0$ and the nonequilibrium dissipation scaling corresponds to $m = 1$ [8–14]. The same analysis leads to a different relation between the exponent a of the wake width and the dissipation exponent m for a self-similar axisymmetric wake [8]. The following conclusions, which were obtained in [7] for the axisymmetric wake, are now also reached for the planar jet: (i) for $m = 0$, $\bar{v}_n \sim \nu/\eta$ where $\eta \equiv (\nu^3/\varepsilon_0)^{1/4}$ is the Kolmogorov length scale provided that $D = 4/3 (= 7/3 - 1$, with $7/3$ being the dimension of the TNTI surface found in [3]), and (ii) for $m = 1$, $\bar{v}_n \sim \nu/\lambda$ where $\lambda^2 \equiv 10\nu K_0/\varepsilon_0$ irrespective of the value of D.

In a region of a planar jet such as $20h \leq x \leq 50h$ where self-similarity coexists with the nonequilibrium dissipation scaling (i.e., $m = 1$), our analysis therefore predicts that the average TNTI speed $\bar{v}_n$ does not scale with the Kolmogorov velocity $v_\eta \equiv \nu/\eta$ but scales, instead, with the Taylor velocity $v_\lambda \equiv \nu/\lambda$. We now proceed to verify this prediction experimentally. To the authors' knowledge, this represents the first investigation of the TNTI propagation speed scaling in a turbulent flow with a wide range of Re_λ values all much higher than 100 (for a list of previous investigations on the topic, see [1]).

The interface propagation speed can be measured by tracking in time an isocontour of the vorticity magnitude [16]. This, however, poses severe challenges, as it requires sufficiently high spatial resolution to correctly sample the interface and at the same time high temporal resolution in order to track in time the propagation of the interface. Another approach, requires the full vorticity vector alongside its spatial derivatives [6], which from an experimental point of view can be extremely challenging due to the effect of the measurement noise. Our approach is based, like our theory, on Eq. (1) and is aimed at the measurement of $\bar{v}_n$. As such, it allows to relax the temporal resolution constraint and does not require spatial derivatives of vorticity.

We perform stereoscopic PIV (stereo-PIV) at four different streamwise locations. A dual cavity or double pulsed Nd:YAG laser (time delay set to 90 μs) illuminates cross sections of the planar jet flow in the y-z planes $x/h = 20, 30, 40, 50$. The two cameras (equipped with 100 mm Macro lenses and Scheimpflug mounts) are located on either sides of the laser, imaging an area extending for $8hx6h$ in the y-z plane, starting from $y = 0$ (Fig. 1).

Equation (1) requires the calculation of the streamwise derivative of the term $\int_{A_\tau} u\,dy\,dz$. We perform this derivative by also acquiring stereo-PIV images at two y-z planes displaced by $\pm 0.3h$ in the x direction from each measurement plane. This results in 4500 images for each plane, which ensures convergence of the relevant statistics.

The cross-correlation is operated using an iterative procedure with a final interrogation window size of 32×32 pixels with 75% overlap. Both raw images and velocity fields are interpolated using spline functions [18]. A Blackman filtering is applied to tune the spatial resolution [19]. The resulting vector pitch is 5η at $x/h = 20$ and reduces to 2.5η at $x/h = 50$.

Our PIV does not have sufficient resolution to calculate turbulence dissipation but as we only need the turbulence dissipation rate ε_0 on the centreline, we use the hot wire anemometry (HWA) measurements carried out in [14]. The turbulence dissipation rate ε_0 was obtained from its isotropic surrogate $15\nu\overline{(\partial u'/\partial x)^2}$ ($u' \equiv u - \langle u \rangle$ is the fluctuating streamwise velocity). Direct numerical simulations ([20]) have shown that the difference between ε_0 and its isotropic surrogate is negligible, particularly on the centreline.

The interface detection from PIV data is often performed by looking at threshold values of the vorticity magnitude or the magnitude of the spanwise vorticity component ω_z. However, the present stereo-PIV data do not provide access to the spanwise vorticity component. Following the approach reported in [21], we look at instantaneous turbulent kinetic energy

$$\tilde{k} = \frac{1}{9U_J^2} \sum_{m,n=-1}^{1} (u_{m,n} - \langle u \rangle)^2 + (v_{m,n})^2 + (w_{m,n})^2, \quad (3)$$

which is a normalized (by U_J^2) average over a 3×3 window ($m = -1, 0, 1$ and $n = -1, 0, 1$) and where the time average $\langle u \rangle$ is calculated at the centre of this 3×3 window. The detection of the interface in terms of $\tilde{k}$ is carried out by trying incremental threshold values k_{thr}. For each of these values, the resulting contour image is discretized in binary levels 0 or 1.

A contour algorithm based on this binary representation is then used to generate contour lines demarcating between regions with level 0 and regions with level 1. These two regions can be separated by more than one continuous line, as patches of one level are often embedded within patches of the other level as illustrated in Fig. 2. We pick as candidate for the TNTI the longest among all the continuous lines on the image.

Watanabe *et al.* [22] demonstrated that isolines based on turbulent kinetic energy thresholds are not faithful representations of the TNTI. They are smoother than vorticity magnitude isolines and less sharply packed together in space for different threshold values. They are therefore not suitable for local measurements of v_n, but can nevertheless be useful for measurements of $\bar{v}_n$ on the basis of Eq. (1), which is valid for any choice of isoline, particularly in the presence of nonequilibrium turbulence dissipation when D does not influence the scaling of $\bar{v}_n$. There is in fact no other alternative at the present high Reynolds numbers where the necessary resolution to accurately capture velocity and vorticity derivatives cannot be achieved.
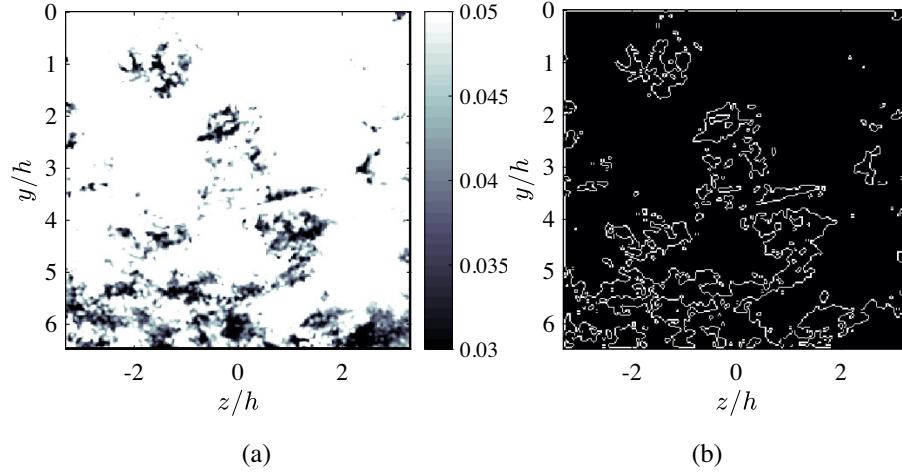
FIG. 2. (a) Contour representation of an instantaneous realization of the flow color coded according to $\tilde{k}$ values. (b) Edge detection using a value of $k_{\text{thr}} = 0.04$. Data are measured at $x/h = 40$.

The next step is to chose the value of k_{thr} which might best represent the average position of the TNTI.

Chauhan *et al.* [21] chose values of k_{thr} leading to a normal distribution of the intermittency function. As the fractal nature of the TNTI is important in our theoretical framework we opt to choose that value of k_{thr} which returns the best-defined fractal dimension D. We therefore apply a box-counting algorithm to the longest continuous line for a given k_{thr} and calculate the average number $N(r)$ of squares of size r needed to cover this curve. This average is calculated over all 1500 instantaneous realizations at the given x/h.

The fractal dimension D exists and is well defined if $N \sim r^{-D}$ over a significant range of scales r. We therefore plot $-\{[d\ln(N)]/[d\ln(r)]\}$ versus $\ln(r/h)$ at all $x/h = 20$, 30, 40, 50 for a wide range of k_{thr} as in Fig. 3(a). This figure shows that, at $x/h = 50$, the isoline with the best-defined

constant $D = -\{[d\ln(N)]/[d\ln(r)]\}$ over a significant range of scales is the one corresponding to $k_{\text{thr}} = 0.04$. Similar plots at $x/h = 20$, 30, 40 show that the isolines with the best-defined D are the ones corresponding to $k_{\text{thr}} = 0.04$ for $x/h = 40$, 50 and $k_{\text{thr}} = 0.035$ for $x/h = 20$, 30. This finalises our choices of k_{thr}.

In Fig. 3(b) we plot $-\{[d\ln(N)]/[d\ln(r)]\}$ versus $\ln(r/h)$ for our chosen isolines at each $x/h = 20$, 30, 40, 50. The fractal dimension turns out to be $D \approx 1.2$ over the approximate range $\lambda \leq r \leq 0.2\delta$ for all $x/h = 20$, 30, 40, 50. It should not be surprising that $D < 4/3$ because, as shown in [22], turbulent kinetic energy isolines are not as irregular as vorticity magnitude isolines and their fractal dimension can therefore be expected to be smaller.

Using the isolines that we selected to represent the TNTI on the basis of their length as continuous lines and of their fractal dimension, we calculate $\mathcal{L}$ and the integral on the
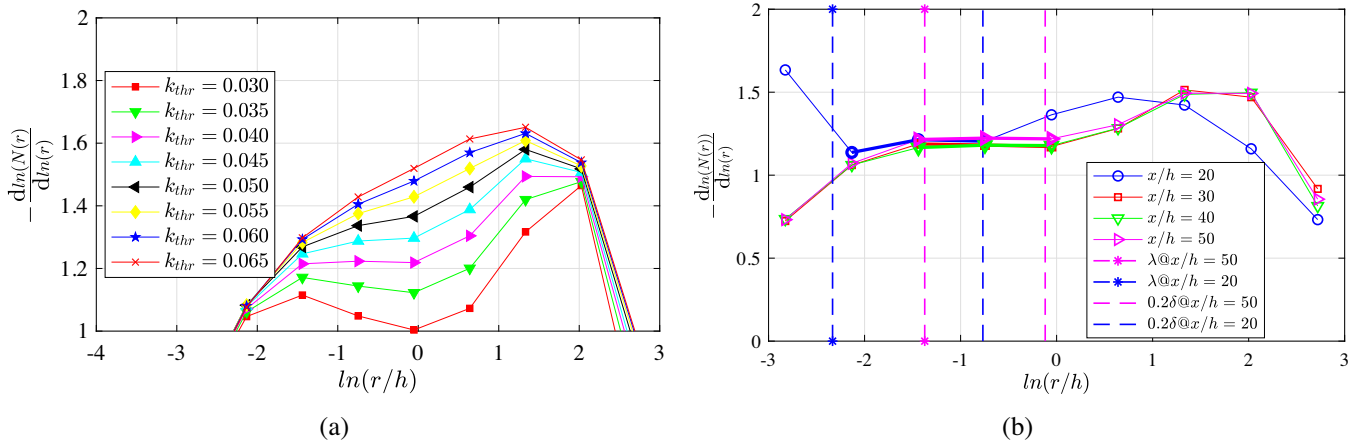

FIG. 3. (a) Plot of $-\{[d\ln(N)]/[d\ln(r)]\}$ versus $\ln(r/h)$ where $N(r)$ is the time-averaged number of squares of size r needed to cover the $\tilde{k} = k_{\text{thr}}$ isoline at $x/h = 50$; data are plotted for different values of the threshold k_{thr}. (b) Same plot but at $k_{\text{thr}} = 0.035$ for $x/h = 20$, 30 and $k_{\text{thr}} = 0.04$ for $x/h = 40$, 50. The vertical dashed lines are representative of the Taylor microscale λ and of 0.2δ (in terms of the jet width δ) at $x/h = 20$ and $x/h = 50$.
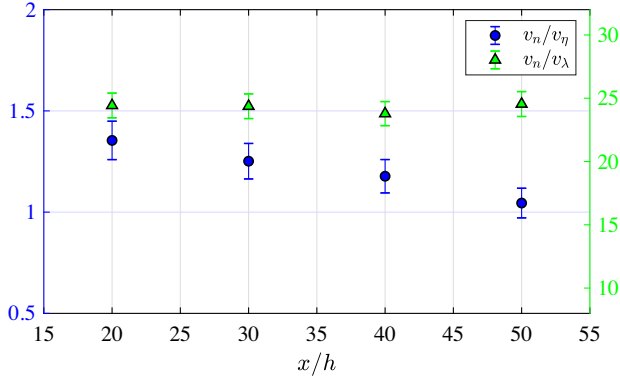
FIG. 4. Ratio of the characteristic TNTI speed $\bar{v}_n$ normalized by the Kolmogorov v_η (full circles and left vertical axis) and by the Taylor velocity v_λ (full triangles and right vertical axis). Error bars indicate 7% of the measured value.

left side of Eq. (1), and we use Eq. (1) to obtain the average TNTI speed $\bar{v}_n$ at positions $x/h = 20, 30, 40, 50$. The results are plotted in Fig. 4: they show that $\bar{v}_n$ scales with the Taylor velocity v_λ and not with the Kolmogorov velocity v_η.

We can also use $D = 1.2$ to indirectly check the Corrsin scaling $\eta_I = \nu/\bar{v}_n$ through the relation $\mathcal{L} \sim 2Z(\eta_I/\delta)^{1-D}$. We therefore calculate the ratio of $\mathcal{L}$ to $2Z(\eta_I/\delta)^{1-D}$ with $\eta_I = \nu/\bar{v}_n$ where $Z = 3h$, given the size of our PIV imaged area (see Fig. 1), and where $\delta(x)$ is taken from the HWA measurements of [14] for the exact same flow at the exact same positions $x/h = 20, 30, 40, 50$. This length ratio is plotted in Fig. 5 and whilst it is close to constant, it exhibits a small rise from $x/h = 20$ to $x/h = 50$. Increasing the range over which one might consider the dimension D to be well defined, from $\lambda \le r \le 0.2\delta$ to $\lambda \le r \le 0.4\delta$, leads to $D \approx 1.25$ rather than $D \approx 1.2$. With this value of D, the ratio of $\mathcal{L}$ to $2Z(\eta_I/\delta)^{1-D}$ becomes much closer to a constant (to within 1.5% of mean value without upward or downward trend) as shown in Fig. 5, thereby supporting Corrsin scaling of the smallest length scale on the interface
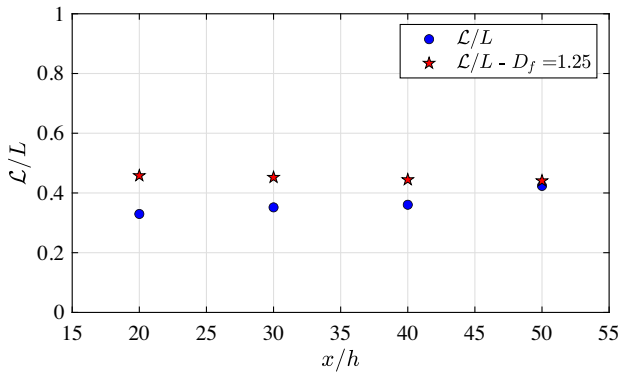
by slightly increasing the fractal range of scales and, as a result, very slightly increasing the fractal dimension D without changing $\bar{v}_n$ (which is still given by Fig. 4).

Conclusions.—In a relatively high Reynolds number region of a turbulent planar jet characterised by the non-equilibrium turbulence dissipation scaling, the average local TNTI speed $\bar{v}_n$ scales with the Taylor velocity $v_\lambda = \nu/\lambda$ rather than the Kolmogorov velocity $v_\eta = \nu/\eta$. We have reached this conclusion from basic theory, and from stereo-PIV measurements in the range of streamwise distances between 20 and 50h where the nonequilibrium turbulence dissipation scaling holds [14].

The present investigation allows for the measurement of the average local TNTI speed on the basis of an averaged approach, which does not rely on high-resolution local propagation velocity measurements at the interface. This has enabled our investigation to reach Reynolds numbers higher than in previous TNTI studies and high enough for the nonequilibrium turbulence dissipation rate scaling to be present within the flow.

The Taylor length λ is an intermediate length which, like η, depends on viscosity but, unlike η, also depends on the turbulent kinetic energy of the turbulence. Most of this energy is in the largest turbulence eddies and potentially in large-scale coherent structures if we are not too far from inlet. In [12,23] it was postulated that the nonequilibrium turbulence dissipation scaling owes its presence to coherent structures. Coherent structures can also be responsible for engulfment [1] and it may be that $\bar{v}_n$ scales with ν/λ when engulfment is an important entrainment mechanism and that $\bar{v}_n$ scales with ν/η when the dominating entrainment mechanism is nibbling [1].

FIG. 5. Ratio $\mathcal{L}/L(\eta_I)$, where $L(\eta_I) = 6h(\eta_I/\delta)^{1-D}$, as a function of streamwise distance x/h, for $D = 1.2$ and $D = 1.25$. The accuracy is $\pm 1\%$.

[*] g.cafiero@surrey.ac.uk
[†] john-christos.vassilicos@centralelille.fr

[1] C. B. da Silva, J. C. Hunt, I. Eames, and J. Westerweel, Annu. Rev. Fluid Mech. **46,** 567 (2014).
[2] J. P. Mellado, Annu. Rev. Fluid Mech. **49,** 145 (2017).
[3] K. R. Sreenivasan, R. R. Prasad, C. Meneveau, and R. Ramshankar, Pure Appl. Geophys. **131,** 43 (1989).
[4] S. Corrsin and A. L. Kistler, NACA Report No. 1244, 1955, p. 1033.
[5] M. Holzner, A. Liberzon, N. Nikitin, B. Lüthi, W. Kinzelbach, and A. Tsinober, J. Fluid Mech. **598,** 465 (2008).

[6] M. Holzner and B. Lüthi, Phys. Rev. Lett. **106**, 134503 (2011).

[7] Y. Zhou and J. C. Vassilicos, J. Fluid Mech. **821**, 440 (2017).

[8] T. Dairay, M. Obligado, and J. C. Vassilicos, J. Fluid Mech. **781**, 166 (2015).

[9] I. P. Castro, J. Fluid Mech. **788**, 1 (2016).

[10] J. C. Vassilicos, Annu. Rev. Fluid Mech. **47**, 95 (2015).

[11] M. Obligado, T. Dairay, and J. C. Vassilicos, Phys. Rev. Fluids **1**, 044409 (2016).

[12] S. Goto and J. C. Vassilicos, Phys. Rev. E **94**, 053108 (2016).

[13] J. Nedić, S. Tavoularis, and I. Marusic, Phys. Rev. Fluids **2**, 032601 (2017).

[14] G. Cafiero and J. C. Vassilicos, Proc. R. Soc. A **475**, 20190038 (2019).

[15] D. K. Bisset, J. C. R. Hunt, and M. M. Rogers, J. Fluid Mech. **451**, 383 (2002).

[16] J. Westerweel, C. Fukushima, J. M. Pedersen, and J. C. Hunt, Phys. Rev. Lett. **95**, 174501 (2005).

[17] J. Westerweel, C. Fukushima, J. M. Pedersen, and J. C. Hunt, J. Fluid Mech. **631**, 199 (2009).

[18] T. Astarita, Exp. Fluids **40**, 977 (2006).

[19] T. Astarita, Exp. Fluids **43**, 859 (2007).

[20] S. A. Stanley, S. Sarkar, and J. P. Mellado, J. Fluid Mech. **450**, 377 (2002).

[21] K. Chauhan, J. Philip, C. M. De Silva, N. Hutchins, and I. Marusic, J. Fluid Mech. **742**, 119 (2014).

[22] T. Watanabe, X. Zhang, and K. Nagata, Phys. Fluids **30**, 035102 (2018).

[23] F. A. Portela, G. Papadakis, and J. C. Vassilicos, Phys. Rev. Fluids **3**, 124609 (2018).

[24] https://www.complete-h2020network.eu/.

Correction: A citation for the website of a supporting project and a statement pertaining to an individual contribution were missing from the Acknowledgments section and have been added. A corresponding reference for the website has been inserted in the reference section.